Asian Research Journal of Mathematics
2(2): 1-23, 2017; Article no.ARJOM.31013

SCIENCEDOMAIN *international*
www.sciencedomain.org

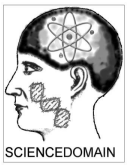

The Effect of Chemical Reaction, and Thermal Radiation on Magnetohydrodynamic Casson Fluid Flow over Non-linearly Stretching Surface with Suction

Bhim Sen Kala[1*]

[1]*K L University, Guntur, 522502, Andhra Pradesh, India.*

Author's contribution

The sole author designed, analyzed and interpreted and prepared the manuscript.

Article Information

DOI: 10.9734/ARJOM/2017/31013
Editor(s):
(1) Palle E. T. Jorgensen, Department of Mathematics, The University of Iowa, Iowa City, Iowa, USA.
Reviewers:
(1) R. Srinivasa Raju, GITAM University, India.
(2) I. G. Baoku, Crescent University, Nigeria.
(3) B. J. Gireesha, Kuvempu University, India.
Complete Peer review History: http://www.sciencedomain.org/review-history/17557

Original Research Article

Received: 14th December 2016
Accepted: 3rd January 2017
Published: 19th January 2017

Abstract

In the present paper, we investigate numerically the effect of chemical reaction, and radiation on magnetohydrodynamic Casson fluid flow over non-linearly stretching surface with fluid suction. By suitable similarity transformations, the governing boundary layer equations are transformed to ordinary differential equations and to solve these equations the method applied is numerical computation with bvp4c, a MATLAB program. The effects of Magnetic, Casson, Stretching index, Suction, Thermal index, Concentration index, chemical reaction and Radiation parameters, and Prandtl number and Schmidth number, on velocity, heat transfer, and concentration profiles, Skin-frictions, Nusselt Number and Sherwood Number are computed and discussed numerically and presented through tables and graphs.

Keywords: Magnetohydrodynamic fluid flow; Casson fluid; radiation parameter; chemical reaction parameter; suction parameter.

**Corresponding author: E-mail: bhimskala@gmail.com;*

NOMENCLATURE AND SI UNITS

μ : *Dynamic viscosity ($kgm^{-2}s^{-1}$)*
υ : *Kinematic viscosity ($m^{-2}s^{-1}$)*
θ : *Dimensionless temperature*
ψ : *Dimentiosless stream function*
B : *Magnetic field (N/(mA))*
h : *Convective heat transfer coefficient (W/m^2K)*
c : *Specific heat (J/kgK)*
Cp : *Specific heat at constant pressure*
D : *Mass diffusivity (m^2s^{-1})*
Gr_T : *Thermal Grashof number*
Grc : *Mass (concentration) Grashof number*
G : *Acceleration due to gravity (ms^{-2})*
k : *Thermal conductivity ($Wm^{-1}K^{-1}$)*
m : *Mass kg*
V : *Volume m^3*
ρ : *Density kg/m^3*
M : *Magnetic parameter*
n : *Stretching index parameter*
Nu : *Local Nusselt number*
Pr : *Prandtl number Prandtl number*
Re : *Local Reynold number*
Sc : *Smidth number*
Sh : *Local Sherwood number*
T : *Temperature of fluid (K)*
C : *Concentration of fluid*
T : *Time(s)*
u : *Horizontal component of velocity (m/s)*
v : *Vertical component of velocity (m/s)*
x : *Distance along the plate distance along the plate*
α : *Thermal diffusivity*
η : *Similarity variable*
x, y : *Cartesian coordianates*
β : *Thermal expansion coefficient (K^{-1})*

1 Introduction

Many natural, industrial as well as biological fluids such as mud, condensed milk, glues, lubricating greases, multi grade oils, gypsum pastes, emulsions, paints, sugar solution, shampoos and tomato paste, ceramics, polymers, liquid detergents, blood, fruit juices etc. change their viscosity or flow behaviour under stress and thus deviate from the classical Newton's law of viscosity. Different models of non-Newtonian fluids based on their diverse flow behaviours have been proposed by the researchers.

The rheological model was introduced originally by Casson [1] in his research on a flow equation for pigment oil-suspensions of printing ink.

Bird et al. [2] investigated the rheology and flow of visco-plastic materials and reported that Casson model constitutes a plastic fluid model which exhibits shear thinning characteristics, yield stress, and high shear viscosity. Casson fluid behaves as solid when the shear stress is less than the yield stress and it starts to deform when shear stress becomes greater than the yield stress.

The fundamental analysis of the flow field of non-Newtonian fluids in a boundary layer adjacent to a stretching sheet or an extended surface is very important and is an essential part in the study of fluid dynamics and heat and mass transfer.

Sakiadis, B. C. [3] studied boundary layer behaviour on continuous solid surfaces: II. The boundary layer on continuous flat surface. Crane L. J. [4] studied the Flow past a stretching plane. Nield, D. A. et al. [5] studied Convection in porous media.

Mukhopadhyay, S [6] investigated Casson fluid flow and heat transfer over a nonlinearly stretching surface. Mustafa, M. et al. [7] studied Model for flow of Casson nanofluid past a non-linearly stretching sheet considering magnetic field effects. Medikare, M. et al. [8] studied MHD Stagnation Point Flow of a Casson Fluid over a Nonlinearly Stretching Sheet with Viscous Dissipation.

Pramanik, S. [9] studied Casson fluid flow and heat transfer past an exponentially porous stretching surface in presence of thermal radiation. Raju, C. S. K. et al. [10] studied Heat and mass transfer in magnetohydrodynamic Casson fluid over an exponentially permeable stretching surface. Saidulu, N. et al. [11] studied Slip Effects on MHD Flow of Casson Fluid over an Exponentially Stretching Sheet in Presence of Thermal Radiation, Heat Source/Sink and Chemical Reaction.

Sharada, K. et al. [12] studied MHD Mixed Convection Flow of a Casson Fluid over an Exponentially Stretching Surface with the Effects of Soret, Dufour, Thermal Radiation and Chemical Reaction. Mukhopadhyay, Swati et al. [13] studied Exact solutions for the flow of Casson fluid over a stretching surface with transpiration and heat transfer effects. Hayat et al. [14] investigated Soret and Dufour effects on magnetohydrodynamic (MHD) flow of Casson fluid. Mahdy, A. [15] studied heat transfer and flow of a Casson fluid due to a stretching cylinder with the Soret and Dufour effects. Animasaun, I. L. [16] studied Effects of thermophoresis, variable viscosity and thermalconductivity on free convective heat and mass transfer of non-Darcian MHD dissipative Casson fluid flow with suction and nth order of chemical reaction.

Ullah, I., Sharidan et al. [17] investigated Effects of slip condition and Newtonian heating on MHD flow of Casson fluid over a nonlinearly stretching sheet saturated in a porous medium.

Reza et al. [18] solved numerically the, boundary layered equations in the work 'Radiation effect on MHD Casson fluid flow over a power-law stretching sheet with chemical reaction' using finite difference method using Thomas algorithm.

Some recent studies concerning the flow, heat and mass transfer analysis of Casson fluid can be found in Refs. [19–46].

In the study of the reference, none of the work concerns with using the MATLAB in-built Numerical Solver bvp4c, to solve boundary layered equations of the work: the effect of chemical reaction, and radiation on magneto hydrodynamic Casson fluid flow over non linearly stretching surface with fluid suction [18].

The present work is based on 'the numerical computation done, using the MATLAB in-built Numerical Solver bvp4c' of boundary layered equations of the work [18].

The accuracy of the results are compare with the works of Ullah et al. [17], Cortell [19], Wang [20], Gorla and Sidawi [21] Khan and Pop [22].

2 Mathematical Formulation of the Problem

In the formulation of the problem we consider following assumptions. Casson fluid is incompressible and electrically conducting. Flow is steady, laminar and two dimensional over a nonlinearly stretching sheet. Flow region is under the influence of transverse magnetic field B. The sheet is stretched nonlinearly along

the x-axis (i.e. y=0) with velocity $u_w(x) = c\,x^n$; origin is taken as fixed and the fluid flow is confined to y>0. Here c is constant and $n(n \geq 0)$ is the nonlinear stretching sheet parameter; $n = 1$ represents the linear sheet case and $n \neq 1$ is for nonlinear case. The magnetic Reynolds number of the flow is taken to be small enough so that induced magnetic field is assumed to be negligible in comparison with applied magnetic field so that $B = (0, B(x), 0)$, where $B(x)$ is the applied magnetic field acting normal to the plate and varies in strength as a function of x. The flow is assumed to be in the x-direction which is taken along the plate and y-axis is normal to it. There is a constant suction/injection velocity v_w normal to the plate.

Under these assumptions the rheological equation for incompressible flow of Casson fluid is given by (Sharada et al. [12], Mukhopadhyay, S., et al. [13]).

$$\tau_{ij} = \begin{cases} 2(\mu_B + p_y / \sqrt{2\pi})e_{ij} & \pi > \pi_c \\ 2(\mu_B + p_y / \sqrt{2\pi_c})e_{ij} & \pi < \pi_c \end{cases},$$

where $\pi = e_{ij}\, e_{ij}$ and e_{ij} is the $(i,i) - \text{th}$ component of the deformation rate , π is the product of the components of deformation , π_c is critical value of the product based on the non-Newtonian model, μ_B is the plastic dynamic viscosity of the non-Newtonian fluid, and p_y is the yield stress of the fluid. The viscosity and thermal conductivity of the fluid are assumed to be constant. There is thermo-diffusion effect as well as diffusion-thermo effect. The pressure gradient, body forces and Joule heating are neglected compared with the effect of viscous dissipation. The temperature and concentration of the stretching surface are always greater than their free stream values. The flow configuration and the coordinate system are shown in Fig. 1.

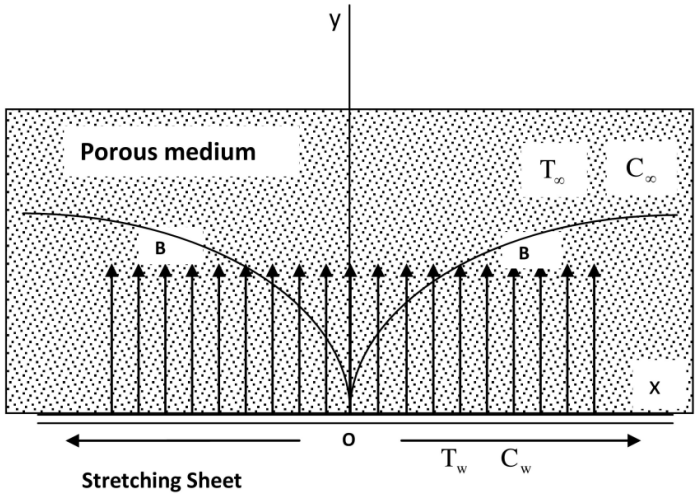

Fig. 1. Physical model and coordinate system

Under the above assumptions and using Bossinesqu approximation, boundary layer equations for flow with heat and mass transfer in Casson fluid (Ullah, I., Sharidan et al. [17]) are given by the following.

The continuity equation:

$$\frac{\partial u}{\partial x}+\frac{\partial v}{\partial y}=0, \tag{1}$$

The equation of momentum:

$$u\frac{\partial u}{\partial x}+v\frac{\partial u}{\partial y}=\upsilon\left(1+\frac{1}{\beta}\right)\frac{\partial^2 u}{\partial y^2}\ -\frac{\sigma B^2(x)}{\rho}u \tag{2}$$

Energy equation:

$$u\frac{\partial T}{\partial x}+v\frac{\partial T}{\partial y}=\frac{k}{\rho C_P}\frac{\partial^2 T}{\partial y^2}\ -\left(\frac{1}{\rho C_P}\right)\frac{\partial q_r}{\partial y} \tag{3}$$

Mass equation:

$$u\frac{\partial C}{\partial x}+v\frac{\partial C}{\partial y}=D\frac{\partial^2 C}{\partial y^2}\ -K(x)(C-C_\infty) \tag{4}$$

where u and v are velocity components along x and y axes, respectively, ρ is fluid density, υ is kinematic viscosity, μ is dynamic viscosity, $\beta=\mu_B\sqrt{2\pi}/p_y$ is the Casson fluid parameter, σ is the electrical conductivity of the fluid and is assumed to be constant, T_W is the temperature of the fluid at the stretching sheet, T is the temperature of the fluid within the boundary layer, T_∞ is the temperature of the fluid outside the boundary layer(free stream temperature), k is the thermal conductivity of the fluid, C_P is the specific heat at constant pressure p, q_r is radiative heat flux, C_W is the concentration of the fluid at the stretching sheet, C is the concentration of the fluid within the boundary layer, C_∞ is the concentration of the fluid outside the boundary layer(free stream concentration), D is the chemical molecular diffusivity. The applied magnetic field is $B = B_0\, x^{\frac{n-1}{2}}$ where B_0 is assumed to be constant.

Boundary conditions:

$$\begin{aligned}&At\ y=0: u=cx^n=U,\quad v=V(x)=V_0\,x^{\frac{n-1}{2}},\\ &T=T_W=T_\infty+T_0\,x^m,\ C=C_W=C_\infty+C_0\,x^t.\\ &As\ y\to\infty: u\to 0,\ T\to T_\infty,\ C\to C_\infty.\end{aligned} \tag{5}$$

c is a parameter related to the surface stretching speed; for surface stretching $c>0$ and for surface shrinking $c<0$. n is the velocity power index related to the surface stretching speed. $V(x)$ is suction velocity; V_0 is constant. T_0 is constant; m is temperature power index parameter. C_0 is constant; t is concentration power index parameter.

The radiative heat flux q_r is simplified by using Rossenland approximation (Bataller, R. C. [30]) as

$$q_r = \frac{4\sigma^*}{3k'}\frac{\partial T^4}{\partial y}. \tag{6}$$

Where σ^* is the Stefan-Boltzmann constant and k' is the mean absorption coefficient.

This approximation is valid at points optically far away from the boundary surface and it is good for intensive absorption, which is for optically thick boundary layer. It is assumed that the temperature difference within the flow is such that the term T^4 may be expressed as a linear function of temperature. Hence expanding T^4 by Taylor's series about T_∞

$$T^4 = T_\infty^4 + 4T_\infty^3(T - T_\infty) + 6T_\infty^2(T - T_\infty)^2 + \ldots \ldots$$

and then neglecting higher order terms beyond the first degree in $(T - T_\infty)$ we get

$$T^4 = 4T_\infty^3 T - 3T_\infty^4 \ .$$

And so

$$q_r = -\left(4\sigma^*/3k^*\right)\left(\partial\left(4T_\infty^3 T - 3T_\infty^4\right)/\partial y\right) = -\left(16\sigma^*/3k^*\right)T_\infty^3\left(\partial T/\partial y\right)$$

And

$$\frac{\partial q_r}{\partial y} = -\frac{16\sigma^* T_\infty^3}{3k^*}\frac{\partial^2 T}{\partial y^2}. \tag{7}$$

Using equations (6) and (7), equation (3) reduces to:

$$\rho C_p\left(u\frac{\partial T}{\partial x} + \upsilon\frac{\partial T}{\partial y}\right) = \left(k + \frac{16\sigma^* T_\infty^3}{3k'}\right)\frac{\partial^2 T}{\partial y^2}. \tag{8}$$

Dimensional Analysis: we define (Ullah, I., Sharidan et al. [17])

$$\begin{gathered}\psi = \left(\frac{2\nu c}{n+1}\right)^{\frac{1}{2}} x^{\frac{n+1}{2}} f(\eta),\ \eta = \left(\frac{c(n+1)}{2\nu}\right)^{\frac{1}{2}} x^{\frac{n-1}{2}} y,\ \theta(\eta) = \frac{(T - T_\infty)}{(T_w - T_\infty)},\ \phi(\eta) = \frac{(C - C_\infty)}{(C_w - C_\infty)}, \\ u = \frac{\partial\psi}{\partial y}, v = -\frac{\partial\psi}{\partial x},\ u = cx^n f'(\eta),\ v = -\left(\frac{c\upsilon(n+1)}{2}\right)^{\frac{1}{2}} x^{\frac{n+1}{2}}\left(f(\eta) + \frac{n-1}{n+1}\eta f'(\eta)\right)\end{gathered} \tag{9}$$

Here η is the similarity variable. ψ is stream function.

Using (9), introducing these variables in the Equations (2), (4) and (8), we get the following dimensionless forms of the equations:

$$(1 + \frac{1}{\beta})f''' + f\,f'' - \frac{2n}{n+1}f'^2 - \frac{2}{n+1}Mf' = 0 \tag{10}$$

$$\left(1+\frac{1}{R}\right)\frac{1}{\Pr}\theta''-\frac{2m}{n+1}f'\theta+f\,\theta'=0 \tag{11}$$

$$\frac{1}{Sc}\phi''-\frac{2t}{n+1}\phi f'+f\phi'-\frac{k_1}{n+1}\phi=0 \tag{12}$$

With parameters:

$$\left.\begin{aligned} &M=\frac{\sigma B_0^2}{\rho c},\Pr=\frac{\upsilon}{k}=\frac{\rho\upsilon C_p}{k}=\frac{\mu C_p}{k},\\ &u=cx^n,\ \nu=\frac{\mu}{\rho},\quad R=\frac{3k\ k'}{16\ \sigma^*\ T_\infty^3}\\ &Sc=\frac{\upsilon}{D},\ K(x)=\frac{cx^{n-1}L}{V_0},\ k1=\frac{2L}{V_0}. \end{aligned}\right\} \tag{13}$$

M is Magnetic parameter (Hartmann number), α is thermal diffusion coefficient, Pr is Prandtl number, D is mass diffusion coefficient, Sc is Schmidth number, $K(x)$ is variable reaction rate, $k1$ is chemical reaction parameter. L is reference length.

And corresponding boundary conditions are as follows:

$$\begin{aligned} &f(0)=S,f'(0)=1,\theta(0)=1,\phi(0)=1\\ &f'(\infty)=0,\ \theta(\infty)=0,\phi(\infty)=0 \end{aligned} \tag{14}$$

Where $$f(0)=-V_0\left(\frac{2}{c\ \upsilon\ (n+1)}\right)^{\frac{1}{2}}=S \tag{15}$$

S is called suction parameter.

The physical quantities of Engineering interest are the Skin friction coefficient (rate of shear stress), the couple stress coefficients at the sheet the Nusselt number (rate of heat transfer), and the Sherwood number (rate of mass transfer).

The local Skin-friction C_f, local Nusselt Number Nu_x and local Sherwood Number Sh_x which are defined as

$$\left.\begin{aligned} &C_f=\frac{\tau_w}{\frac{\rho U_w^2}{2}}=\frac{\mu_B\left(1+\frac{1}{\beta}\right)\left(\frac{\partial u}{\partial y}\right)_{y=0}}{\frac{\rho U_w^2}{2}}\Rightarrow C_f=\left(\frac{2\nu(n+1)}{c}\right)^{\frac{1}{2}}x^{-\frac{(n+1)}{2}}f''(0),\\ &C_f=\left(\frac{2(n+1)}{\mathrm{Re}}\right)^{\frac{1}{2}}\left(1+\frac{1}{\beta}\right)f''(0),\ \mathrm{Re}=\frac{cx^{(n+1)}}{\nu}. \end{aligned}\right\} \tag{16}$$

$$\left.\begin{aligned} Nu &= -\frac{x\left(\frac{\partial T}{\partial y}\right)_{y=0}}{T_w - T_\infty} = -\left(\frac{c(n+1)}{2\nu}\right)^{\frac{1}{2}} x^{\frac{(n+1)}{2}} \theta'(0), \\ Nu &= -\left(\frac{(n+1)cx^{(n+1)}}{2\nu}\right)^{\frac{1}{2}} \theta'(0) = -\left(\frac{(n+1)}{2}\mathrm{Re}\right)^{\frac{1}{2}} \theta'(0). \end{aligned}\right\} \tag{17}$$

Here $-\left(\frac{\partial T}{\partial y}\right)_{y=0}$ is a heat flux from the surface of the sheet and Re is the local Reynold Number.

$$\left.\begin{aligned} Sh &= -\frac{x\left(\frac{\partial C}{\partial y}\right)_{y=0}}{C_w - C_\infty} = -\left(\frac{c(n+1)}{2\nu}\right)^{\frac{1}{2}} x^{\frac{(n+1)}{2}} \phi'(0), \\ Sh &= -\left(\frac{(n+1)cx^{(n+1)}}{2\nu}\right)^{\frac{1}{2}} \phi'(0) = -\left(\frac{(n+1)}{2}\mathrm{Re}\right)^{\frac{1}{2}} \phi'(0). \end{aligned}\right\} \tag{18}$$

Here $-\left(\frac{\partial C}{\partial y}\right)_{y=0}$ is a mass flow rate from the surface of the sheet and Re is the local Reynold Number.

3 Method of Numerical Solution

The numerical solutions are obtained using the equations (10)-(12) and boundary conditions (14) for some values of the governing parameters, namely, Magnetic parameter (M), Casson parameter (b), Stretching Index parameter (n1), Suction parameter (S), Prandtl number (Pr), Radiation parameter(R), Schmidth number (Sc), Thermal index parameter (m), Concentration index parameter(t), and Chemical reaction parameter(k_1) on the steady boundary layer flow are discussed in detail. The numerical computation is done using the MATLAB in-built Numerical Solver bvp4c. In the computation we have taken $\eta_\infty = 12$ and axis according to the clear figure-visuality.

4 Results Analysis and Discussion

In order to analyze the behaviour of non-dimensional linear velocity $f'(\eta)$, temperature $\theta(\eta)$, and concentration $\phi(\eta)$ profiles of the physical problem, numerical calculations are carried out for various values of Magnetic parameter (M), Casson parameter (b), Stretching Index parameter(n1), Suction parameter (S), Prandtl number(Pr), Radiation parameter (R), Schmidth number (Sc), Thermal index parameter (m), Concentration index parameter (t), and Chemiocal reaction parameter (c). Also, the Skin-friction, Nusselt and Sherwood numbers are discussed. For illustrations of the results, the numerical data are tabulated in Tables 1-13 and plotted in Figs. 2–19.

The results for skin friction and local Nusselt number and reduced Nassult numbers are compared with the previous published results, and are shown in Tables 1–3. It is observed that the obtained results are in good agreement with the published results.

Tables 1, 2 and 3 present the values of skin friction coefficient and local Nassult number, and reduced Nusselt number for different values of nonlinear stretching parameter n and Prandtl number Pr, respectively. The present results are compared with the results of Ullah et al. [17], Cortell [19], Wang [20], Gorla and Sidawi [21], Khan and Pop [22].

It is also observed from Table 1 that magnitude of skin friction coefficient $\left|\left(1+\frac{1}{b}\right)f''(0)\right|$ increases with the increase in n1 and Table 2 shows local Nusselt number decreases with the increase in n1 and increases with increase in Pr.

Table 3 shows the comparison of the present results for reduced Nusselt number with various values of Pr with the results of Wang [20], Gorla and Sidawi [21] and Khan and Pop [22]. It is found that the rate of heat transfer coefficient increases as Pr increases.

For the convenience in calculation in Matlab following symbles are used for respective symbols used in modelling equations and boundary conditions:

$$M = Magnetic\ \ parameter,\ b = \beta\ \ Casson\ \ Parameter,\ n1 = n\ \ Stretchin index\ parameter,$$
$$S = Suction\ parameter,\ \ \Pr = \Pr andtl\ \ number,\ R = Radiation\ \ parameter$$
$$Sc = Schmidth number,\ c = Chemical reaction\ parameter\ \ k_1,$$
$$m = Thermal\ \ index\ parameter, t = Concentration\ \ index\ \ parameter,$$

Table 1. Comparison of $-f''(0)$ for different values of n1 with M=0; n1=1; b=10.^8; Pr=1; R=inf; t=0; m=0; Sc=0.22; S=0.0; c=0;

M=0; n1=1; b=10.^8; Pr=1; R=inf; t=0; m=0; Sc=0.22; S=0.0; c=0;			
		$-f''(0)$	
n1	**Cortell [19]**	**Ullah et al. [17]**	**Present**
0.0	0.627547	0.6276	0.627554111495105
0.2	0.766758	0.7668	0.766835311872827
0.5	0.889477	0.8896	0.889537395487564
1	1.0	1.0	1.000001131721189
3	1.148588	1.1486	1.148604214083713
10	1.234875	1.2349	1.234882849405469
100	1.276768	1.2768	1.276784084458797

The effect of M is illustrated in Fig. 2. All the trajectories are of same family with the magnetic number in between 0 and 3. It is seen that fluid velocity reduces as M increases. It is due to the fact that drag force, also known as Lorentz force is produced when magnetic field is applied to the fluid. This force has the tendency to slow down the velocity of fluid in the boundary layer. The decreasing pattern of velocity field with the increase in similarity variable shows that transverse magnetic field opposes the transport phenomenon. Thus the momentum boundary layer thickness decreases as M increases.

It is seen in Fig. 3 that the temperature profile increases with increasing magnetic parameter and causes thickening of the corresponding boundary layer.

It is seen in Fig. 4 that the concentration profile increases with increasing Magnetic parameter and causes thickening of the corresponding boundary layer.

Table 2. Comparison of local Nassult number $-\theta'(0)$, for different values of n1 with M=0; n1=0.2; b=10.^8; Pr=1 and 5; R=inf; t=0; m=0; Sc=0.22; S=0.0; k_1=0;

M=0; n1=0.2; b=10.^8; R=inf; t=0; m=0; Sc=0.22; S=0.0; c=0; $-\theta'(0)$, Pr=1,				M=0; n1=0.2; b=10.^8; R=inf; t=0; m=0; Sc=0.22; S=0.0; c=0; $-\theta'(0)$, Pr=5,		
n1	**Cortell [19]**	**Ullah et al. [17]**	**Present**	**Cortell [19]**	**Ullah et al. [17]**	**Present**
0.2	0.610262	0.6102	0.610203981361	1.607175	1.6076	1.607799764754
0.5	0.595277	0.5949	0.595204129502	1.586744	1.5868	1.586794023622
1.5	0.574537	0.5747	0.574736444244	1.557463	1.5576	1.557705129027
3.0	0.564472	0.5647	0.564671395375	1.542337	1.5430	1.543190746978

Table 3. Comparison of results for reduced Nassult number $-\theta'(0)$, for different values of Pr with M=0; n1=1; b=10.^8; Pr=0.7; R=inf; t=0; m=0; Sc=0.22; S=0.0; c=0;

M=0; n1=1; b=10.^8; Pr=0.7; R=inf; t=0; m=0; Sc=0.22; S=0.0; c=0; $-\theta'(0)$, Pr=1,					
Pr	**Wang [20]**	**Gorla and Sidawi [21]**	**Khan and Pop [22]**	**Ullah et al. [17]**	**Present**
0.7	0.4539	0.5349	0.4539	0.4544	0.454049789569805
2	0.9114	0.9114	0.9113	0.9113	0.911361122074545
7	1.8954	1.8905	1.8954	1.8953	1.895415847905391
20	3.3539	3.3539	3.3539	3.3538	3.353940662862386
70	6.4622	6.4622	6.4621	6.4638	6.462331549437675

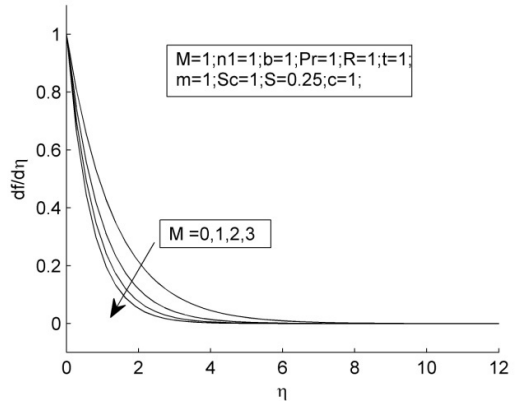

Fig. 2. Velocity profile $f'(\eta)$ with respect to similarity transformation η for some values of Magnetic parameter M

Fig. 5 shows that velocity profile decreases with the decrease in the values of Casson parameter and this causes decrease in corresponding boundary layer thickness.

Fig. 6 shows the temperature profile increases with the increase in Casson parameter and this causes increase in corresponding boundary layer thickness.

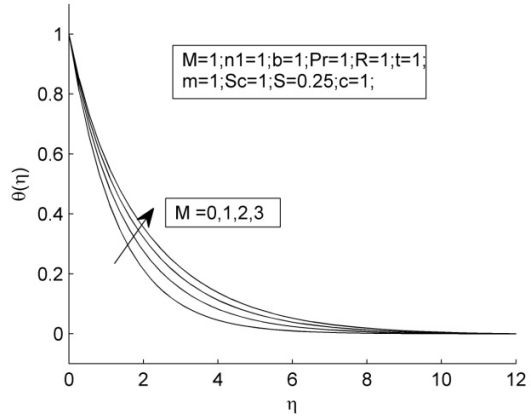

Fig. 3. Temperature profile $\theta(\eta)$ with respect to η for some values of Magnetic parameter M

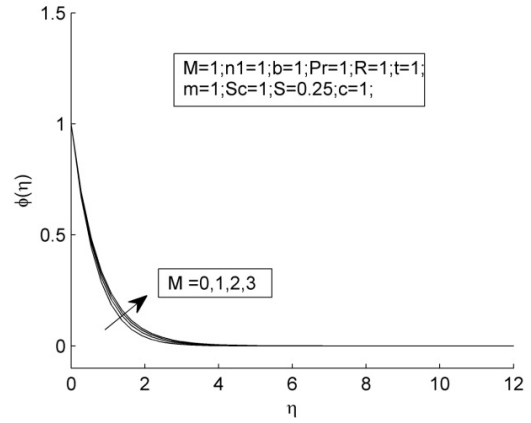

Fig. 4. Concentration profile $\phi(\eta)$ with respect to η for some values of Magnetic parameter M

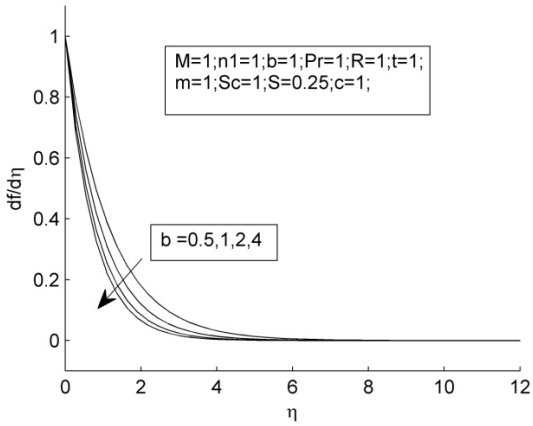

Fig. 5. Velocity profile $f'(\eta)$ with respect to similarity transformation η for some values of Casson parameter b

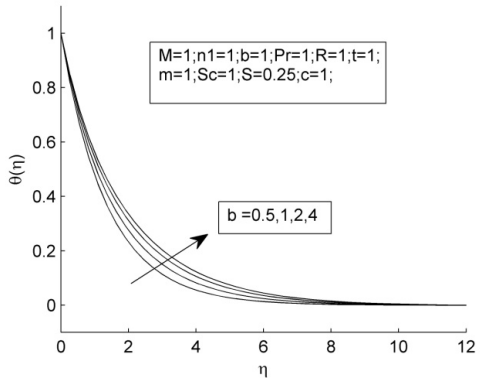

Fig. 6. Temperature profile $\theta(\eta)$ with respect to η for some values of Casson parameter b

Fig. 7 shows the concentration profile increases with the increases with the increase in Casson parameter and thus causes increase is corresponding boundary layer thickness.

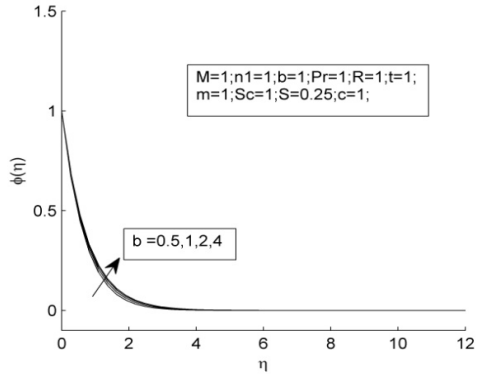

Fig. 7. Concentration profile $\phi(\eta)$ with respect to η for some values of Casson parameter b

Fig. 8 shows the velocity profile decreases with the increase in stretching index parameter and thus causes decrease in corresponding boundary layer thickness.

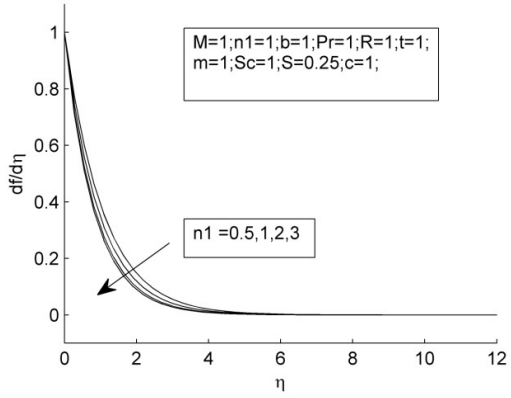

Fig. 8. Velocity profile $f'(\eta)$ with respect to similarity transformation η for some values of stretching index parameter n1

Fig. 9 shows the temperature profile increases with the increase in stretching index parameter and thus causes increase in corresponding boundary layer thickness.

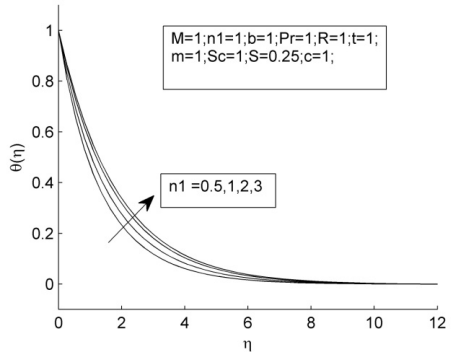

Fig. 9. Temperature profile $\theta(\eta)$ with respect to η for some values of stretching index parameter

Fig. 10 shows the concentration profile increases with the increase in stretching index parameter and thus causes increase in corresponding boundary layer thickness.

Fig. 11 shows the velocity profile decreases with the increase in suction parameter and thus causes decrease in corresponding boundary layer thickness.

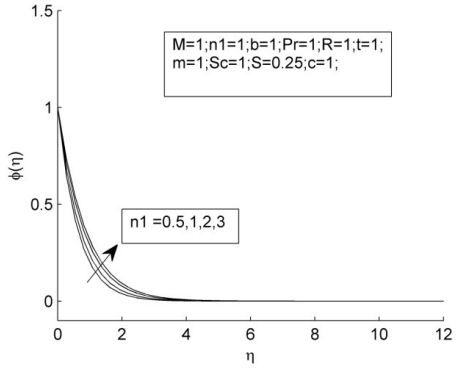

Fig. 10. Concentration profile $\phi(\eta)$ with respect to η for some values of stretching index parameter n1

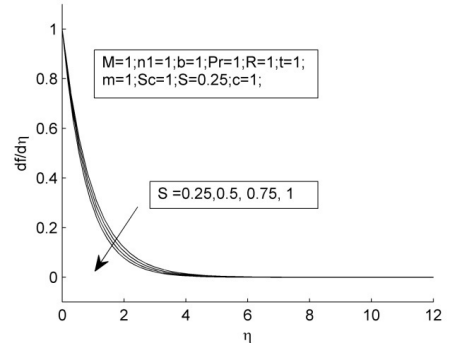

Fig. 11. Velocity profile $f'(\eta)$ with respect to similarity transformation η for some values of Suction parameter S

Fig. 12 shows the temperature profile decreases with the increase in suction parameter and thus causes decrease in corresponding boundary layer thickness.

Fig. 13 shows the concentration profile decreases with the increases in suction parameter S, and thus causes decrease in corresponding boundary layer thickness.

Fig. 14 shows the temperature profile decreases with the increases in Thermal index parameter m, and thus causes corresponding decreases in boundary layer thickness.

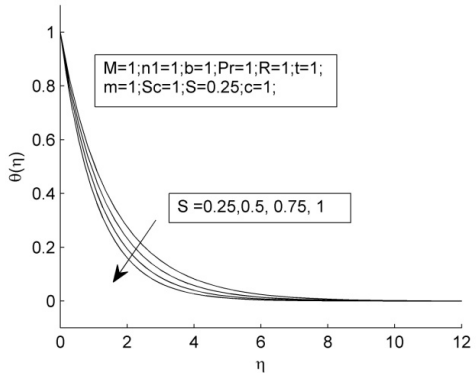

Fig. 12. Temperature profile $\theta(\eta)$ with respect to η for some values of Suction parameter S

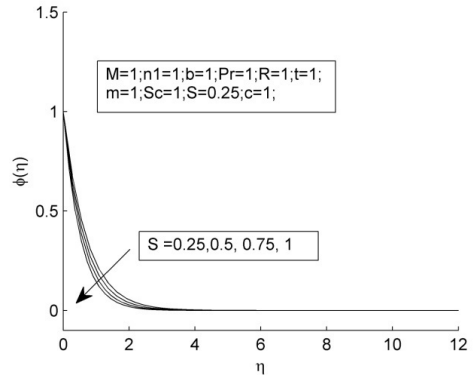

Fig. 13. Concentration profile $\phi(\eta)$ with respect to η for some values of Suction parameter S

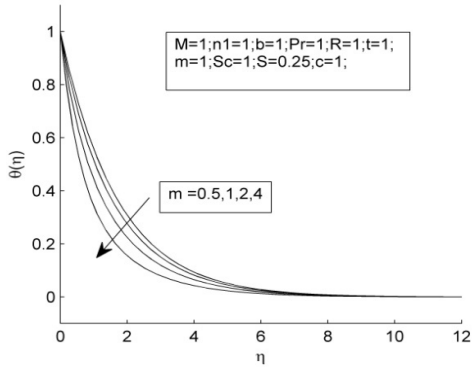

Fig. 14. Temperature profile $\theta(\eta)$ with respect to η for some values of thermal index parameter m

Fig. 15 shows the temperature profile decreases with the increases in Prandtl number and thus causes decreases in corresponding boundary layer thickness.

Fig. 16 shows the temperature profile decreases with the increases in Radiation parameter R, and thus causes decreases in corresponding boundary layer thickness.

Fig. 17 shows the concentration profile decreases with the increases in Schmidth number Sc, and thus causes decreases in corresponding boundary layer thickness.

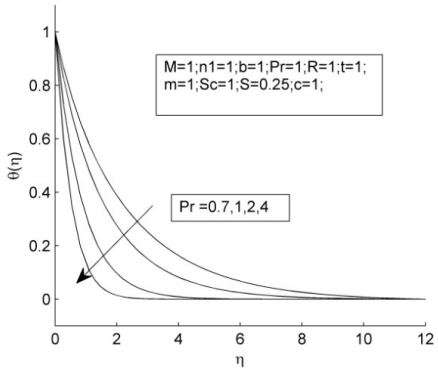

Fig. 15. Temperature profile $\theta(\eta)$ with respect to η for some values of Prandtl number Pr

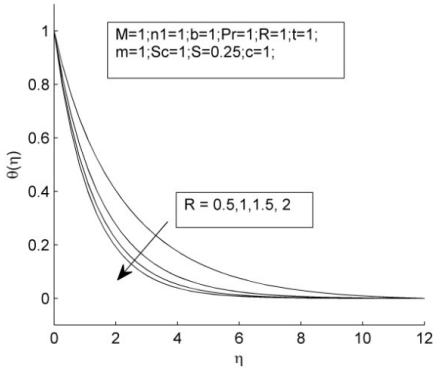

Fig. 16. Temperature profile $\theta(\eta)$ with respect to η for some values of radiation parameter R

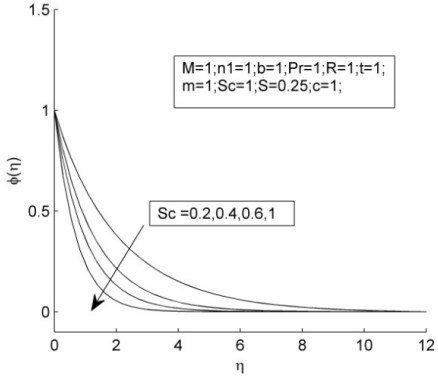

Fig. 17. Concentration profile $\phi(\eta)$ with respect to η for some values of Smidth parameter Sc

Fig. 18 shows the concentration profile decreases with the increase in the value of Chemical reaction parameter c, and thus causes decrease in corresponding boundary layer thickness.

Fig. 19 shows the concentration profile decreases with the increases in the value of Concentration Index parameter t, and thus causes decreases in corresponding boundary layer thickness.

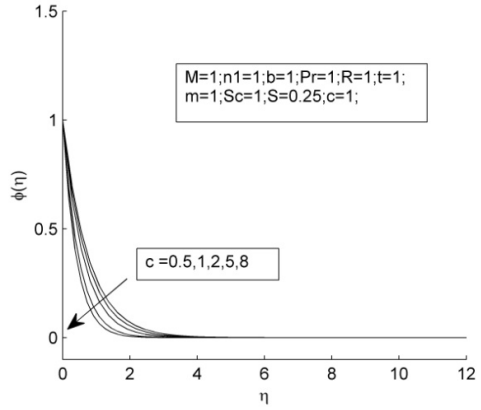

Fig. 18. Concentration profile $\phi(\eta)$ with respect to η for some values of chemical reaction parameter c

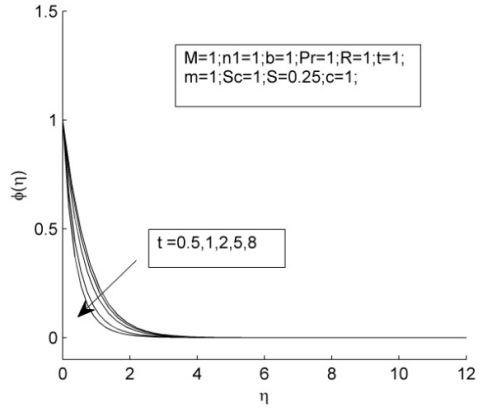

Fig. 19. Concentration profile $\phi(\eta)$ with respect to η for some values of concentration index parameter t

Table 4 shows with the increase in Magnetic parameter (M), Skin -friction, Nusselt number and Sherwood number decrease.

Table 5 shows with the increase in Casson parameter (b), Skin -friction, Nusselt number and Sherwood number decrease.

Table 6 shows with the increase in Stretching Index parameter (n1), Skin -friction, Nusselt number and Sherwood number decrease.

Table 4. Comparison of local Skin-friction $f''(0)$, Nusselt number $-\theta'(0)$, and Sherwood number $-\phi'(0)$ for various values of Magnetic parameter M

M=1; n1=1; b=1; Pr=1; R=1; t=1; m=1; Sc=1; S=0.25; c=1;			
M	$f''(0)$	$-\theta'(0)$	$-\phi'(0)$
0	-0.772380765882430	0.772380765882400	1.443691334729526
1	-1.064451227933708	0.703353442961857	1.397884038796368
2	-1.288838554005237	0.654907768407752	1.365372722305526
3	-1.478093956613316	0.617912526785317	1.339875593768916

Table 5. Comparison of local Skin-friction $f''(0)$, Nusselt number $-\theta'(0)$, and Sherwood number $-\phi'(0)$ for various values of Casson parameter b

M=1; n1=1; b=1; Pr=1; R=1; t=1; m=1; Sc=1; S=0.25; c=1;			
b	$f''(0)$	$-\theta'(0)$	$-\phi'(0)$
0.5	-0.859225894421490	0.751334137204969	1.429688788817794
1	-1.064451227933708	0.703353442961857	1.397884038796368
2	-1.241036996916409	0.664825218572031	1.372092721488271
4	-1.368857754042093	0.638820030080323	1.354376225410678

Table 6. Comparison of local Skin-friction $f''(0)$, Nusselt number $-\theta'(0)$, and Sherwood number $-\phi'(0)$ for various values of Stretching Index parameter n1

M=1; n1=1; b=1; Pr=1; R=1; t=1; m=1; Sc=1; S=0.25; c=1;			
n1	$f''(0)$	$-\theta'(0)$	$-\phi'(0)$
0.5	-0.918105532143194	0.810336626979573	1.578794600600632
1	-1.064451227933708	0.703353442961857	1.397884038796368
2	-1.192839815888933	0.600512982322554	1.201288066348144
3	-1.252024024566633	0.550357874663092	1.094265501542168

Table 7. Comparison of local Skin-friction $f''(0)$, Nusselt number $-\theta'(0)$, and Sherwood number $-\phi'(0)$ for various values of Suction parameter S

M=1; n1=1; b=1; Pr=1; R=1; t=1; m=1; Sc=1; S=0.25; c=1;			
S	$f''(0)$	$-\theta'(0)$	$-\phi'(0)$
0.25	-1.064451227933708	0.703353442961857	1.397884038796368
0.5	-1.132782222290359	0.781250513161171	1.548889097761843
0.75	-1.204926289151033	0.864402649566321	1.710870598067398
1.0	-1.280776407766019	0.952182976893372	1.882814891094115

Table 7 shows with the increase in Suction parameter(S), Skin -friction decreases, Nusselt number and Sherwood number increase.

Table 8 shows with the increase in Thermal power Index parameter (m), Skin -friction first increases and then decreases, Nusselt number increases and Sherwood number first decreases and then increases.

Table 8. Comparison of local Skin-friction $f''(0)$, Nusselt number $-\theta'(0)$, and Sherwood number $-\phi'(0)$ for various values of Temperature power index parameter m

M=1; n1=1; b=1; Pr=1; R=1; t=1; m=1; Sc=1; S=0.25; c=1;			
m	$f''(0)$	$-\theta'(0)$	$-\phi'(0)$
0.5	-1.064451228004112	0.579972075082871	1.397884039133279
1	-1.064451227933708	0.703353442961857	1.397884038796368
2	-1.064451229001629	0.922520745033117	1.397884051444187
4	-1.064451229007984	1.285239044709142	1.397888512222279

Table 9 shows with the increase in Prandtl number (Pr), Skin –friction first increases and then decreases, Nusselt number and Sherwood number increase.

Table 10 shows with the increase in Radiation parameter (R), Skin -friction first increases and then decreases, Nusselt number and Sherwood number increase.

Table 9. Comparison of local Skin-friction $f''(0)$, Nusselt number $-\theta'(0)$, and Sherwood number $-\phi'(0)$ for various values of parameter Pr

M=1; n1=1; b=1; Pr=1; R=1; t=1; m=1; Sc=1; S=0.25; c=1;			
Pr	$f''(0)$	$-\theta'(0)$	$-\phi'(0)$
0.7	-1.064451227935287	0.539046293903134	1.397884038793309
1	-1.064451227933708	0.703353442961857	1.397884038796368
2	-1.064451229001544	1.148963683105466	1.397884051475590
4	-1.064451229007306	1.828562782440114	1.397884279456529

Table 10. Comparison of local Skin-friction $f''(0)$, Nusselt number $-\theta'(0)$, and Sherwood number $-\phi'(0)$ for various values of Radiation parameter R

M=1; n1=1; b=1; Pr=1; R=1; t=1; m=1; Sc=1; S=0.25; c=1;			
R	$f''(0)$	$-\theta'(0)$	$-\phi'(0)$
0.5	-1.064451227935287	0.519510958603281	1.397884038793309
1.0	-1.064451227933708	0.703353442961857	1.397884038796368
1.5	-1.064451229000330	0.803015948852864	1.397884051476741
2.0	-1.064451229000330	0.865904761663387	1.397884051476745

Table 11 shows with the increase in Smidth number (Sc), Skin -friction first increases and then decreases, and Nusselt number first decreases and then increases, and Sherwood number increases.

Table 11. Comparison of local Skin-friction $f''(0)$, Nusselt number $-\theta'(0)$, and Sherwood number $-\phi'(0)$ for various values of Schmidth parameter Sc

M=1; n1=1; b=1; Pr=1; R=1; t=1; m=1; Sc=1; S=0.25; c=1;			
Sc	$f''(0)$	$-\theta'(0)$	$-\phi'(0)$
0.2	-1.064451227307101	0.703353431798897	0.517087265237630
0.4	-1.064451227305958	0.703353429832318	0.795180570166533
0.6	-1.064451227306725	0.703353431000844	1.021457499285938
1.0	-1.064451227933708	0.703353442961857	1.397884038796368

Table 12 shows with the increase in Chemical reaction parameter (c), Skin -friction first increases and then decreases, and Nusselt number first decreases and then increases and Sherwood number increase.

Table 12. Comparison of local Skin-friction $f''(0)$, Nusselt number $-\theta'(0)$, and Sherwood number $-\phi'(0)$ for various values of Chemical reaction parameter c

M=1; n1=1; b=1; Pr=1; R=1; t=1; m=1; Sc=1; S=0.25; c=1;			
c	$f''(0)$	$-\theta'(0)$	$-\phi'(0)$
0.5	-1.064451227935144	0.703353444895451	1.282872003805204
1	-1.064451227933708	0.703353442961857	1.397884038796368
2	-1.064451228001790	0.703353444160419	1.595139951113721
5	-1.064451228799512	0.703353036214121	2.055987515833043

Table 13 shows with the increase in Concentration power index (t), Skin -friction, Nusselt number decrease and Sherwood number increases.

Table 13. Comparison of local Skin-friction $f''(0)$, Nusselt number $-\theta'(0)$, and Sherwood number $-\phi'(0)$ for various values of Concentration power index parameter t

M=1; n1=1; b=1; Pr=1; R=1; t=1; m=1; Sc=1; S=0.25; c=1;			
t	$f''(0)$	$-\theta'(0)$	$-\phi'(0)$
0.5	-1.064451227932965	0.703353443754825	1.246986619289261
1	-1.064451227933708	0.703353442961857	1.397884038796368
2	-1.064451228585952	0.703353100846418	1.671140561168520
5	-1.064451229008724	0.703353060524090	2.340352375400558

5 Conclusion

In the present work we studied the effect of chemical reaction, and radiation on magnetohydrodynamic Casson fluid flow over non-linearly stretching surface with fluid suction. The effects of Magnetic, Casson, and Prandtl number, Radiation parameters and Schmidth number, Chemical reaction parameter, Stretching index, Suction, Thermal index, and Concentration index parameters on velocity, heat transfer, and concentration profiles, Skin-friction, Nusselt Number and Sherwood Number are computed and discussed numerically and presented through tables and graphs. From the work following conclusion are obtained.

1. With the increase in the values of Magnetic parameter, Cassson parameter Suction parameter, the velocity profile decreases, and this causes decrease in corresponding boundary layer thickness.
2. With the increase in Magnetic parameter, Cassson parameter, Stretching index parameter, the temperature profile increases and thus causes increase in corresponding boundary layer thickness.
3. With the increase Magnetic parameter, Cassson parameter, Stretching index parameter, the concentration profile increases with the increase in stretching index parameter and thus causes increase in corresponding boundary layer thickness.
4. With the increases in Prandtl number, Radiation parameters, Suction parameter, Thermal index parameter, the temperature profile decreases, and thus causes decreases in corresponding boundary layer thickness.
5. With the increases in the value of Schmidth number, Chemical reaction parameter, Suction parameter, concentration index parameter, the concentration profile decreases, and thus causes decreases in corresponding boundary layer thickness.

6. Skin -friction first increases and then decreases, with the increase in the value of Prandtl number, Radiation parameters, Schmidth number, Chemical reaction parameter, Thermal index parameter, each.
7. Skin -friction decreases, with the increase in the value of Magnetic parameter, Casson fluid parameter, stretching index parameter, Suction parameter, concentration index parameter, each.
8. Nassult number increases, with the increase in the value of Prandtl number, Radiation parameters, Suction parameter, Thermal index parameter.
9. Nassult number first decreases and then increases, with the increase in the value of Schmidth number, Chemical reaction parameter, each.
10. Nassult number decreases, with the increase in the value of Magnetic parameter, Casson fluid parameter, stretching index parameter, concentration index parameter, each.
11. Sherwood number increases, with the increase in the value of Suction parameter, Prandtl parameter, Radiation parameter, Schmidth parameter, Chemical reaction parameter, concentration index parameter, each.
12. Sherwood number first decreases and then increases with the increase in Thermal power Index parameter.
13. Sherwood number decreases, with the increase in the value of Magnetic parameter, Casson fluid parameter, stretching index parameter, each.

Competing Interests

Author has declared that no competing interests exist.

References

[1] Casson N. In: Mill CC, editor. A flow equation for pigment oil-suspensions of the printing ink type. Rheology of Disperse Systems, 84. Pergamon Press; 1959.

[2] Bird RB, Dai GC, Yarusso BJ. The rheology and flow of viscoplastic materials. Rev Chem Eng. 1983;1(1):36-69.

[3] Sakiadis BC. Boundary layer behavior on continuous solid surfaces: II. The boundary layer on continuous flat surface. AIChE J. 1961;7:221–225.

[4] Crane LJ. Flow past a stretching plane. Z. Angew. Math. Phys. 1970;21:645–647.

[5] Nield DA, Bejan A. Convection in porous media. 2nd ed. Springer, New York; 1999.

[6] Mukhopadhyay Swati. Casson fluid flow and heat transfer over a nonlinearly stretching surface. Chin. Phys. B. 2013;22(7):074701.
DOI: 10.1088/1674-1056/22/7/074701

[7] Mustafa M, Junaid Ahmad Khan. Model for flow of Casson nanofluid past a non-linearly stretching sheet considering magnetic field effects. AIP Advances. 2015;5:077148.
Available: http://dx.doi.org/10.1063/1.4927449

[8] Medikare M, Joga S, Chidem KK. MHD stagnation point flow of a Casson fluid over a nonlinearly stretching sheet with viscous dissipation. American Journal of Computational Mathematics. 2016;6: 37-48.
Available: http://dx.doi.org/10.4236/ajcm.2016.61005

[9] Pramanik S. Casson fluid flow and heat transfer past an exponentially porous stretching surface in presence of thermal radiation. Ain Shams Engineering Journal. 2014;5:205–212.
Available: http://dx.doi.org/10.1016/j.asej.2013.05.003

[10] Raju CSK, Sandeep N, Sugunamma V, Jayachandra Babu M, Ramana Reddy JV. Heat and mass transfer in magnetohydrodynamic Casson fluid over an exponentially permeable stretching surface. Engineering Science and Technology, an International Journal. 2016;19:45–52.
Available: http://dx.doi.org/10.1016/j.jestch.2015.05.010

[11] Saidulu N, Venkata Lakshmi A. Slip effects on MHD Flow of Casson fluid over an exponentially stretching sheet in presence of thermal radiation, heat source/sink and chemical reaction. European Journal of Advances in Engineering and Technology. 2016;3(1):47-55.

[12] Sharada K, Shankar B. MHD mixed convection flow of a Casson fluid over an exponentially stretching surface with the effects of Soret, Dufour, thermal radiation and chemical reaction. World Journal of Mechanics. 2015;5:165-177.
Available: http://dx.doi.org/10.4236/wjm.2015.59017

[13] Swati Mukhopadhyay, Krishnendu Bhattacharyya, Tasawar Hayat. Exact solutions for the flow of Casson fluid over a stretching surface with transpiration and heat transfer effects. Chin. Phys. B. 2013;22(11):114701.
DOI: 10.1088/1674-1056/22/11/114701

[14] Hayat T, Shehzadi SA, Alsaedi A. Soret and Dufour effects on magnetohydrodynamic (MHD) flow of Casson fluid. Appl Math Mech (English Ed.). 2012;33(10):1301–12.

[15] Mahdy A. Heat transfer and flow of a Casson fluid due to a stretching cylinder with the Soret and Dufour effects. Journal of Engineering Physics and Thermophysics. 2015;88:4.

[16] Animasaun IL. Effects of thermophoresis, variable viscosity and thermal conductivity on free convective heat and mass transfer of non-darcian MHD dissipative Casson fluid flow with suction and nth order of chemical reaction. Journal of the Nigerian Mathematical Society. 2015;34:11–31.
Available: http://dx.doi.org/10.1016/j.jnnms.2014.10.008

[17] Imran Ullah, Sharidan Shafie, Ilyas Khan. Effects of slip condition and Newtonian heating on MHD flow of Casson fluid over a nonlinearly stretching sheet saturated in a porous medium. Journal of King Saud University –Science. j.jksus; 2016.
Available: http://dx.doi.org/10.1016

[18] Motahar Reza, Rajni Chahal, Neha Sharma. Radiation effect on MHD Casson fluid flow over a power-law stretching sheet with chemical reaction, world academy of science, engineering and technology. International Journal of Chemical, Molecular, Nuclear, Materials and Metallurgical Engineering. 2016;10:5.

[19] Cortell R. Viscous flow and heat transfer over a nonlinearly stretching sheet. Appl. Math. Comput. 2007;184:864–873.

[20] Wang CY. Free convection on a vertical stretching surface. J. Appl. Math. Mech. (ZAMM). 1989;69: 418–420.

[21] Gorla RSR, Sidawi I. Free convection on a vertical stretching surface with suction and blowing. Appl. Sci. Res. 1994;52:247–257.

[22] Khan WA, Pop I. Boundary-layer flow of a nanofluid past a stretching sheet. Int. J. Heat Mass Transf. 2010;53:2477–2483.

[23] Shehzad SA, Hayat T, Qasim M, Asghar S. Effects of mass transfer on MHD flow of Casson fluid with chemical reaction and suction. Brazilian Journal of Chemical Engineering. 2013;30(01):187-195.

[24] Arthur EM, Seini IY, Bortteir LB. Analysis of Casson fluid flow over a vertical porous surface with chemical reaction in the presence of magnetic field. Journal of Applied Mathematics and Physics. 2015;3:713-723.
Available: http://dx.doi.org/10.4236/jamp.2015.36085

[25] Hussanan Abid, Mohd Zuki Salleh, Razman Mat Tahar, Ilyas Khan. Unsteady boundary layer flow and heat transfer of a Casson fluid past an oscillating vertical plate with Newtonian heating. PLOS ONE. 2014;9(10):e108763.
Available: www.plosone.org

[26] Kirubhashankar CK, Ganesh S, Mohamed Ismail A. Casson fluid flow and heat transfer over an unsteady porous stretching surface. Applied Mathematical Sciences. 2015;9(7):345–351.
Available: http://dx.doi.org/10.12988/ams.2015.411988

[27] Motahar Reza, Rajni Chahal, Neha Sharma. Radiation effect on MHD Casson fluid flow over a power-law stretching sheet with chemical reaction. World Academy of Science, Engineering and Technology. International Journal of Chemical, Molecular, Nuclear, Materials and Metallurgical Engineering. 2016;10:5.

[28] Siddiqui AM, Farooq AA, Rana MA. A mathematical model for the flow of a Casson fluid due to metachronal beating of cilia in a tube. Hindawi Publishing Corporation's Scientific World Journal; 2015. Article ID 487819, 12 pages.
Available: http://dx.doi.org/10.1155/2015/487819

[29] Shaw Sachin, Ganeswar Mahanta, Precious Sibanda. Non-linear thermal convection in a Casson fluid flow over a horizontal plate with convective boundary condition. Alexandria Engineering Journal. 2016;55:1295–1304.
Available: http://dx.doi.org/10.1016/j.aej.2016.04.020

[30] Rao AS, Prasad VR, Reddy NB, B´eg OA. Heat transfer in a Casson rheological fluid from a semi-infinite vertical plate with partial slip. Wiley Periodicals, Inc. Heat Trans Asian Res; Published Online in Wiley Online Library; 2013.
Available: http://dx.doi.org/10.1002/htj.21115

[31] Forchheimer PZ. Wasserbewegung Durch Boden. Zeit Ver Deutsch Ing. 1901;45:1781–8.

[32] Darcy H. Les fontainer publigues de la ville de Dijoin. Dalmont; 1856.

[33] Butt AS, Tufail MN, Asif Ali. Three-dimensional flow of a magnetohydrodynamic Casson fluid over an unsteady stretching sheet embedded into a porous medium. Journal of Applied Mechanics and Technical Physics. 2016;57(2):283–292. c_ Pleiades Publishing, Ltd.; 2016.
ISSN: 0021-8944.

[34] Bataller RC. Radiation effects in the Blasius flow. Appl. Math. Comp. 2012;198:333-338.

[35] Srinivasa Raju R, Jithender Reddy G, Anand Rao J, Rashidi MM, Rama Subba Reddy Gorla. Analytical and numerical study of unsteady MHD free convection flow over an exponentially moving vertical plate with heat absorption. International Journal of Thermal Sciences. 2016;107:303–315.

[36] Srinivasa Raju R, Jitthender Reddy G, Anand Rao J, Rashidi MM. Thermal diffusion and diffusion thermo effects on an unsteady heat and mass transfer MHD natural convection Couette flow using FEM. Journal of Computational Design and Engineering. 2016;3(4):349–362.
DOI: 10.1016/j.jcde.2016.06.003

[37] Srinivasa Raju R. Effects of Soret and Dufour on natural convective fluid flow past a vertical plate embedded in porous medium in presence of thermal radiation via FEM. Journal of the Korean Society for Industrial and Applied Mathematics. 2016;20(4):309–332.

[38] Srinivasa Raju R, Anil Kumar M, Dharmendar Reddy Y. Unsteady MHD free convective flow past a vertical porous plate with variable suction. ARPN Journal of Engineering and Applied Sciences. 2016;11(23):13608–13616.

[39] Srinivasa Raju R, Venkatesh N, Anil Kumar M, Jithender Reddy G. Influence of transpiration on unsteady heat transfer MHD fluid flow over an infinite vertical plate in presence of hall current. ARPN Journal of Engineering and Applied Sciences. 2016;11(23):14008–14013.

[40] Jitthender Reddy G, Srinivasa Raju R, Anand Rao J. Thermal diffusion and diffusion thermo impact on chemical reacted MHD free convection from an impulsively started infinite vertical plate embedded in a porous medium using FEM. Journal of Porous Media; 2016. (In press)

[41] Ramya Dodda, Srinivasa Raju R, Anand Rao J. Numerical simulation of MHD boundary layer partial slip flow of nanofluids over a nonlinear stretching sheet with suction/injection. Journal of Nanofluids; 2016. (In press)

[42] Sailaja SV, Shanker B, Srinivasa Raju R. Double diffusive effects on MHD mixed convection Casson fluid flow towards a vertically inclined plate filled in porous medium in presence of biot number: A finite element technique. Journal of Nanofluids; 2016. (In press)

[43] Jitthender Reddy G, Srinivasa Raju R, Anand Rao J, Rama Subba Reddy Gorla. Unsteady MHD couette flow of water at 4^{o}C in a rotating system in presence of heat transfer with ramped temperature via finite element method. International Journal of Applied Mechanics and Engineering; 2016. (In press)

[44] Srinivasa Raju R. Influence of angle of inclination on unsteady MHD Casson fluid flow past a vertical surface filled by porous medium in presence of constant heat flux, chemical reaction and viscous dissipation. Journal of Nanofluids; 2016. (In press)

[45] Krishnamurthy MR, Gireesha BJ, Prasannakumara BC, Gorla Rama Subba Reddy. Thermal radiation and chemical reaction effects on boundary layer slip flow and melting heat transfer of nanofluid induced by a nonlinear stretching sheet. Nonlinear Engineering. 2016;5(3):147-159.
DOI: 10.1515/nleng-2016-0013

[46] Prasannakumara BC, Gireesha BJ, Gorla Rama SR, Krishnamurthy MR. Effects of chemical reaction and nonlinear thermal radiation on Williamson nanofluid slip flow over a stretching sheet embedded in a porous medium. Journal of Aerospace Engineering. 2016;29:5.

Peer-review history:
The peer review history for this paper can be accessed here (Please copy paste the total link in your browser address bar)
http://sciencedomain.org/review-history/17557